Hindawi
Advances in Civil Engineering
Volume 2022, Article ID 5306923, 14 pages
https://doi.org/10.1155/2022/5306923

Research Article

Numerical Simulation of the Stability of a Cutting Slope and Study on Its Reinforcement Scheme

Song Chen[1,2] **Zhao Yang**[3] **Wenpeng Zhang**[2,4] **Liufang Li**[5] **Yibo Zheng**[1,2] **and Ying Yuan**[2,4]

[1]*Hebei Key Laboratory of Optoelectronic Information and Geo-detection Technology, Hebei GEO University, Shijiazhuang 050031, China*
[2]*College of Urban Geology and Engineering, Hebei GEO University, Shijiazhuang 050031, China*
[3]*Guangdong Hualu Transport Technology Co., Ltd., Guangzhou 510420, China*
[4]*Hebei Technology Innovation Center for Intelligent Development and Control of Underground Built Environment, Hebei GEO University, Shijiazhuang 050031, China*
[5]*College of Civil Engineering and Mechanics, Lanzhou University, Lanzhou 730000, China*

Correspondence should be addressed to Liufang Li; lliufun@126.com

Received 14 July 2022; Accepted 3 September 2022; Published 5 October 2022

Academic Editor: Ziyu Tao

Analyzing the stability of the slope and studying the reinforcement scheme can reduce ecological disasters, improve the ecological environment, and protect people's lives and property. In this paper, taking the left side slope of ZK100 + 860~+975 cutting of the Huizhou-Qingyuan section of the Shantou-Zhanjiang Expressway as an example, based on the strength reduction method (SRM), the stability of the slope under different conditions (natural conditions, unsupported excavation conditions, rainstorm conditions, and reinforcement conditions) is analyzed by using finite element software. The results show that the slope was almost stable before excavation, and the safety factor of slope stability decreases due to excavation, so it is in an unstable state. Rainwater has a great influence on the stability of the slope. The damage to the slope is deepened, and the stability safety factor is decreased under the rainstorm condition. The stability safety factor of the slope has increased by 24.3% after the reinforcement of the anchor rod and anchor cable, and the slope is in a stable state. It can be seen that the anchor rod and anchor cable can effectively control the deformation of the slope and have a good reinforcement effect.

1. Introduction

At present, there are many common methods to analyze slope stability, including the slice method, rigid body limit equilibrium method, plastic limit analysis method [1], stereographic projection method, and strength reduction method (SRM). However, the ideal method to truly analyze slope stress, deformation, and stability is the strength reduction method (SRM) [2]. The strength reduction method (SRM) was introduced into slope stability analysis in the 1960s. Later, in order to make it more suitable for engineering practice and study the failure mechanism and characteristics of the slope, many scholars in China conducted in-depth research on this basis. Yuan et al. proposed a new nonlinear SRM method based on the generalized Hoek-Brown (GHB) criterion, which provides a reduction strategy with precise physical significance for seeking the optimal parameter set of rock slope failure [3]. Wang et al. put forward a discrete element modeling method (DSDM) for the stability of jointed rock slopes based on displacement statistics on the basis of the strength reduction method (SRM), which can be coupled with anti-SRM to effectively analyze the stability of jointed slopes with potential sliding surfaces [4]. Yang et al., considering the nonlinear failure characteristics of rock mass, proposed 3D-NSRNMM based on the nonlinear GHB failure criterion to conduct a 3D analysis of rock slope to study the stability of slope [5]. Nie et al. used the constant boundary element method to discretize sliding mass to study SRM-related slope instability criteria and got a relatively reliable conclusion [6]. Sun et al.,

based on the incremental method of elastic-plastic mechanics and bilinear projection operator method, combined the strength reduction method with φ-ν inequality and proposed a virtual element strength reduction technique to analyze the stability of slope [7]. Zhou and Hua combined rock mechanics theory, nonlinear finite element analysis technology, and the strength reduction coefficient method to put forward the strength parameter reduction finite element method, which can effectively analyze the stability of bedding rock cutting slope [8]. Chen et al. put forward a dynamic stability evaluation method for slopes based on the dynamic and overall strength reduction method and carried out stability evaluation and support analysis of slopes [9]. Some scholars combine the strength reduction method with the limit equilibrium method to quantitatively analyze the slope and evaluate its stability [10–12]. Based on the above research findings, with the in-depth study of slope problems, the finite element strength reduction method has become the mainstream method to analyze the stress, displacement, and stability of slopes, and a series of new slope research methods have been derived based on its basic principles.

In the existing cases of slope stability analysis based on the finite element strength reduction method (SRM), some scholars only consider the impact of excavation on slope stability [13–15] while ignoring the impact of heavy rainfall. Studies have shown that heavy rainfall is also one of the most important factors affecting slope stability [16]. Based on this statement, many scholars have carried out extensive research. Sun et al. used the saturated-unsaturated strength and infiltration theory of silty sand slopes to study the influence of rainfall infiltration on slope stability by numerical simulation [17]. Tian et al. obtained the soil mechanical parameters of the slope through triaxial compression, saturated infiltration and other geotechnical tests and, based on this, established a finite element model to study the stability of the slope with rainfall intensity and duration [18]. Song and Tan conducted a large number of indoor rainfall tests combined with DIC image technology to explore the failure mechanism of the soil slope under heavy rainfall and finally obtained the failure characteristics of the slope in different scenarios [16]. In terms of rock and soil material properties, Bai et al. [19–21] have studied the particle interaction and mutual coupling mechanisms of rock and soil, which play a certain key role in slope stability.

The research in this paper is based on the principle of the finite element strength reduction method (SRM). Taking a specific slope project as an actual case, the natural and excavation conditions of the slope are quantitatively analyzed by Midas software. At the same time, take heavy rainfall into account, study the impact of rainfall on the slope, and put forward the slope support design scheme according to the actual engineering needs. This provides a basis for studying the stability of slopes under different working conditions, solving practical construction problems, and optimizing support design schemes.

2. Project Background

The Huizhou-Qingyuan section of the Shantou-Zhanjiang Expressway is located in the central part of Guangdong Province. The project route starts at Hengcha Village, Longhua Town, Longmen County, Huizhou City, crosses the *T*-shape of the Guanghe Expressway, and ends at Taihe Town, Qingxin District, Qingyuan City, connecting with the Qingyuan-Yunfu section of the Shantou-Zhanjiang Expressway, with a total length of 126200.0 m. The project is located on the left side of ZK100 + 860 ~ ZK100 + 975 cutting, with a slope length of 115.0 m and a maximum slope height of 50.0 m. This place is located in the hills, where the terrain fluctuates greatly. The ground elevation of the slope is about 154.2~186.2 m, and the natural slope angle is about 25~30°. The mainline map and slope topographic map are shown in Figure 1.

According to the drilling data and field geological mapping results, the slope rocks are mainly quaternary colluvial silty clay, Yanshanian granite and its weathered layer. The quaternary overburden and all strongly weathered layers of the slope are thick, the vegetation is well developed, and no joints are measured in the slope area. The section of structural plane occurrence is shown in Figure 2. The climate in this area is mild, the rainfall is abundant, and the surface runoff has a great impact on the foot of the slope. Atmospheric precipitation is the main source of groundwater supply. According to the drilling data, the buried depth of the underground stable water level is about 21m, measured locally in the drilling depth, while others are not found. Relevant parameters of slopes and stages at all levels after excavation on the left side are shown in Table 1.

3. Numerical Simulation of Slope Stability

3.1. Finite Element Software and Method. MIDAS GTS NX is a commonly used finite element numerical simulation software in geotechnical engineering, which is usually suitable for modeling tunnels, slopes, and other projects. It can be used for linear dynamic analysis, seepage and consolidation analysis, etc., and can simulate many special working conditions for complex operations. The finite element model of the slope is established in Midas, and the stability safety factor of the slope is calculated by the strength reduction method. The strength reduction method (SRM) is a common method to calculate F_s (the safety factor) of slope stability. The basic principle is that the shear strength indexes c and φ of soil continuously reduce until the slope is in the critical state of limit equilibrium. The specific calculation formula is as follows:

$$c' = \frac{c}{F_s},$$

$$\tan\varphi' = \frac{\tan\varphi}{F_s}, \tag{1}$$

$$\tau' = c' + \sigma\tan\varphi'.$$

Matters that need attention are as follows: (1) the initial value of the reduction coefficient and the increment of F_s should be small enough to ensure the numerical calculation result and (2) the value of the reduction coefficient before divergence is the stability safety factor of the slope.

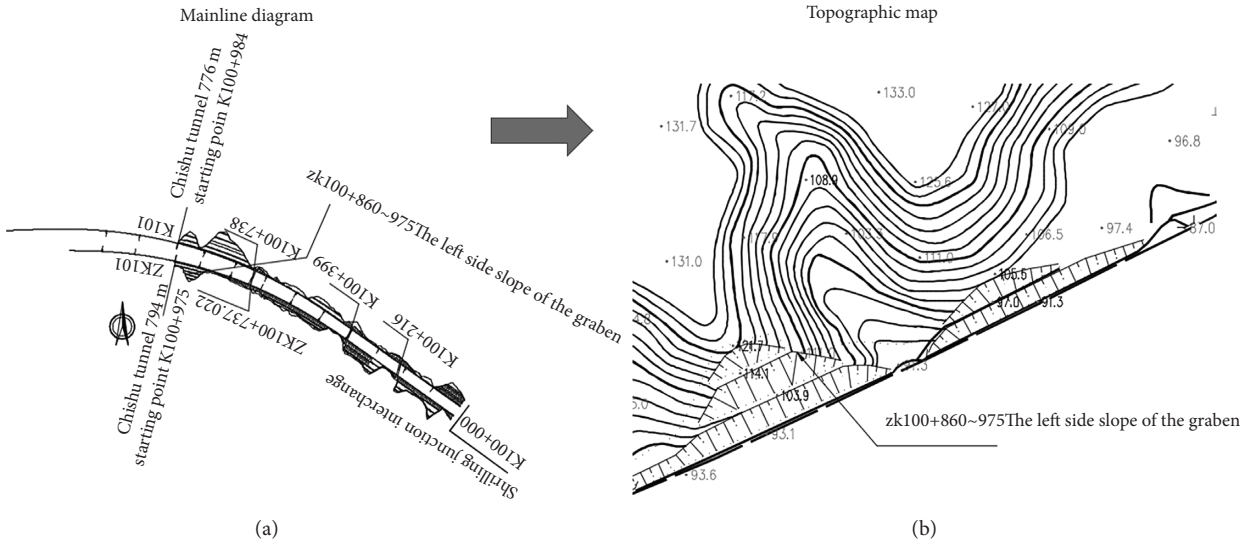

Figure 1: Mainline map (a) and topographic map of the left side slope of cutting (b).

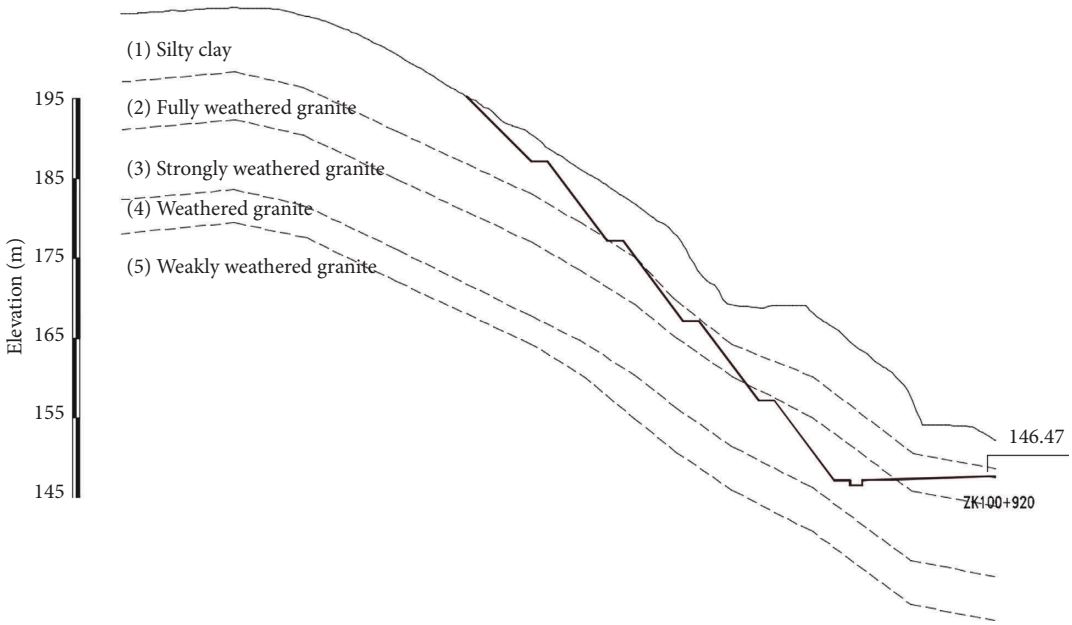

Figure 2: Geological profile of slope.

3.2. Selection of Instability Criterion. There are three main criteria for judging slope instability by finite element strength reduction method:

(1) The plastic zone of the slip surface is completely connected [22]

(2) The displacement and strain on the slip surface suddenly change, resulting in a very large and unlimited plastic flow [23]

(3) Double convergence criterion of force and displacement; judging from the convergence criterion of force and displacement, the model calculation is not convergent

3.3. Numerical Model and Parameters. According to the geological profile and construction excavation scheme, the finite element calculation model is established. There are two types of models: one is the model under natural conditions, and the other is the stratum model after excavation, as shown in Figure 3.

The two models are 151 meters long and 100 meters high. According to automatic mesh generation, the natural model is divided into 12116 units and 12364 nodes. The excavation model is divided into 11178 units and 11389 nodes. The boundary condition of the tectonic geostress field should be considered at the bottom and left and right sides of the model and the whole model should be loaded with self-

Table 1: Table of parameters related to slope excavation.

Slope stage	Slope ratio	Height (m)	Width (m)
The 1st slope stage	1 : 0.75	10	2
The 2nd slope stage	1 : 0.75	10	2
The 3rd slope stage	1 : 0.75	10	2
The 4th slope stage	1 : 0.75	10	2
The 5th slope stage	1 : 1.00	Varies	—

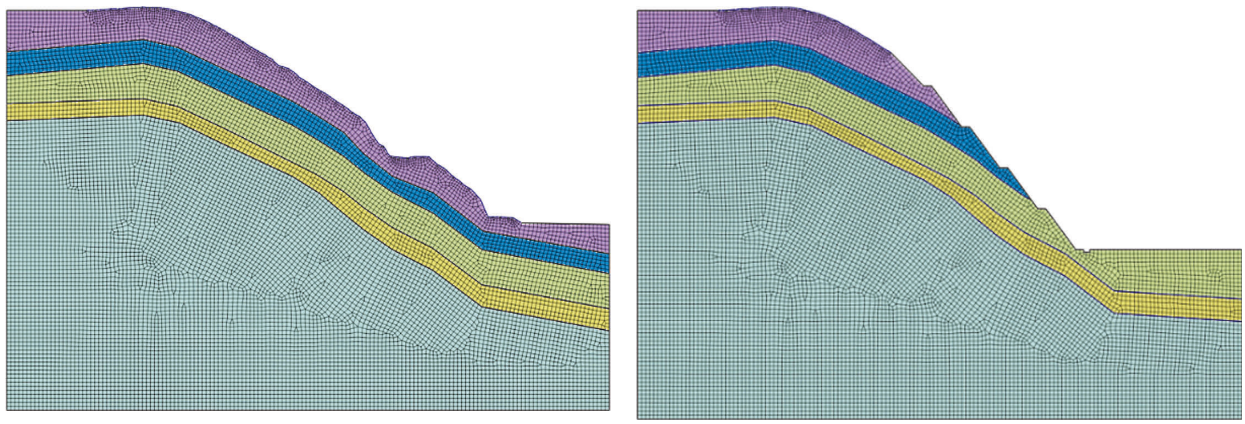

(a) (b)

Figure 3: Numerical calculation model. (a) Model in natural state. (b) The model after excavation.

weight stress. Considering the rock mass attribute characteristics of strata, Mohr–Coulomb constitutive model is selected as the model grid material, and the specific physical and mechanical parameters of rock mass materials are shown in Table 2.

3.4. Result Analysis

3.4.1. The Condition under Natural Conditions. The strength reduction method (SRM) is used to calculate the safety and stability coefficient of the slope model under natural conditions. The results show that the value is 1.05, the slip surface is not penetrated, and the slope is in an unstable state.

As shown in Figure 4, according to the displacement-stress contour, the displacement in the middle and upper parts of the slope is the largest, with the maximum displacement reaching 0.0932 m, where the rock strata are severely deformed and often heave. At this position, the downward deformation along the slope shows a decreasing trend until the bottom of the slope, the displacement of the rock stratum is minimal, and almost no deformation occurs. The effective plastic strain contour is shown in Figure 5, and the results show that the maximum strain in the plastic region is 0.0246, and the slip surface in the slope extends from the top to the foot of the slope, but there is no penetration. The length of the slip surface is about to 86 m, and it exists in an arc shape at the interface between silty clay and granite strata. The overall slip-crack effect is very obvious, and the shear outlet is located at the foot of the slope.

3.4.2. The Condition of Excavation Without Support. According to the Revit stratum map, after excavation, a finite element model is established, and boundary conditions are imposed. On this basis, the strength reduction method is used to calculate the slope stability. The results show that the safety factor of slope stability decreases to 0.97 after grade 5 excavation, and the plastic zone of the slip surface has been completely penetrated. At this time, the slope is unstable.

Figure 6 shows the displacement contour. It can be seen from the figure that the large displacement and deformation of the slope after excavation are mostly concentrated at the fourth and fifth slopes, and the maximum displacement is about 0.113 m, while the displacement and deformation of the first, second, and third slopes are relatively small, which can be ignored by comparison.

The effective plastic strain contour is shown in Figure 7. According to the analysis, the slip zone is about 45 m long, distributed between 4.5 and 8 m below the slope, and the maximum plastic strain of the slope is 0.0322. Compared with the natural condition, the slip surface is shorter in length, and the shear outlet position becomes the platform between the fourth and fifth slopes.

3.5. Influence of Rainfall Infiltration on Slope Stability.

The slope is located in an area with abundant rain and rainy days all year round. In order to study the degree of influence of rain on slope stability, numerical simulation software is used to simulate and analyze the influence of rain on slope stability.

Table 2: Physical parameters of rock mass materials.

Name	C (kPa)	φ (°)	Young's modulus (MPa)	Poisson's ratio	Natural gravity (kN/m^3)
Silty clay	19	18	40	0.3	18
Completely weathered granite	25	25	31000	0.15	19
Highly weathered granite	28	29	40000	0.22	21
Moderately weathered granite	31	32	55000	0.36	22
Weakly weathered granite	32	33	60000	0.37	23

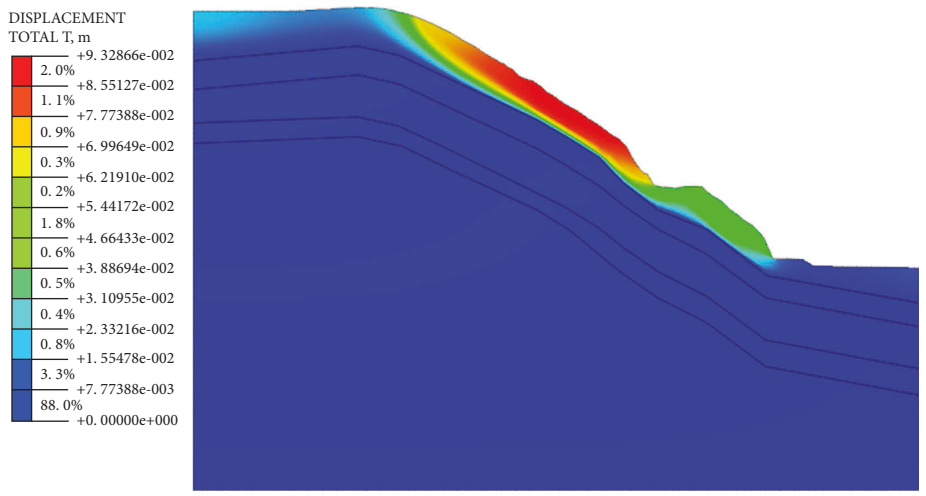

Figure 4: Contour of displacement under natural conditions.

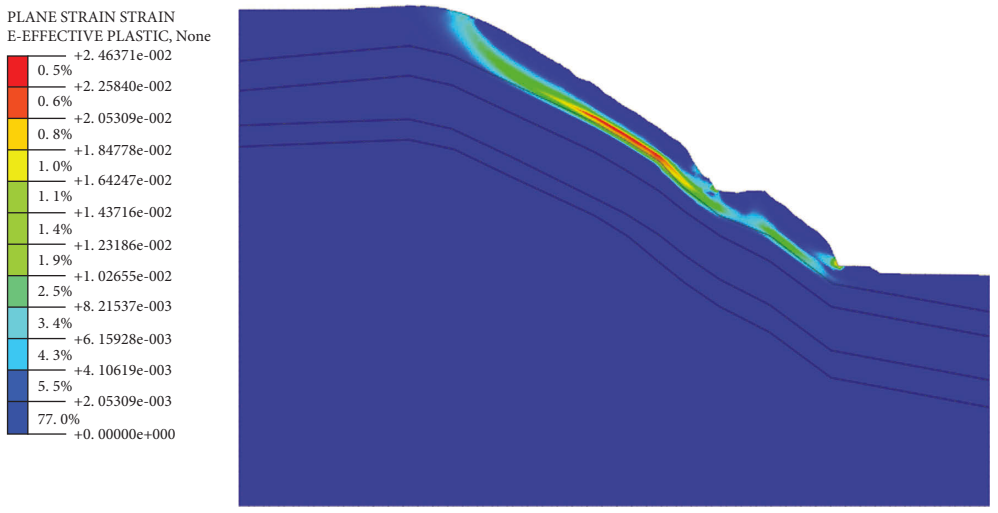

Figure 5: Contour of effective plastic strain under natural conditions.

In this paper, based on the excavated slope model, when establishing the model, according to the soil data in Table 2, the corresponding material attributes are given to each stratum. The permeability and water-bearing function of the material is defined by the van Genuchten model, and the specific characteristic curves are shown in Figures 8 and 9. The expression is

$$\theta = \theta_r + \frac{\theta_s - \theta_r}{\left[1 + (a \times h)^n\right]^m}, \quad m = 1 - \frac{1}{n}, \tag{2}$$

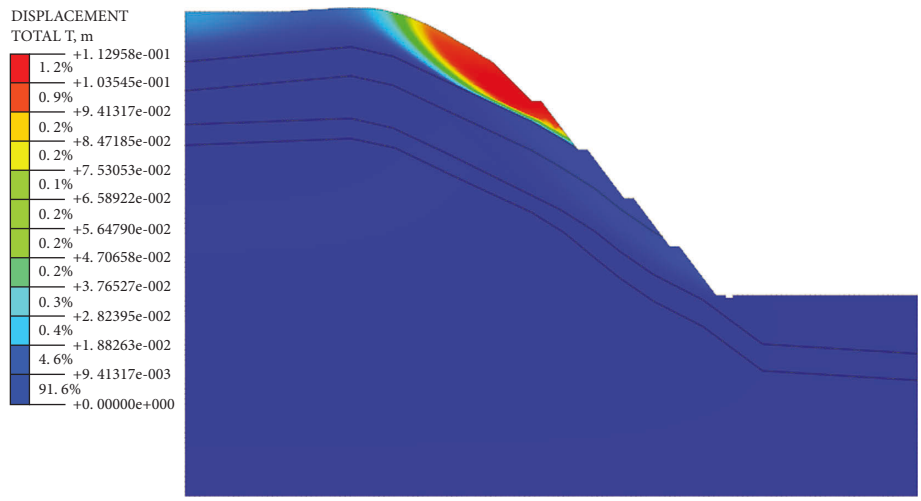

Figure 6: Displacement contour under the condition of excavation without support.

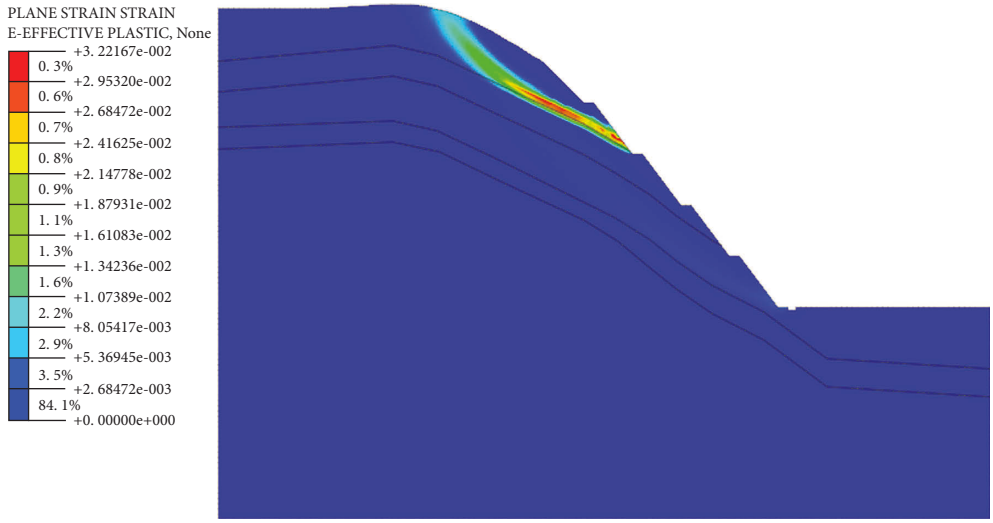

Figure 7: Contour of effective plastic strain under excavation and unsupported conditions.

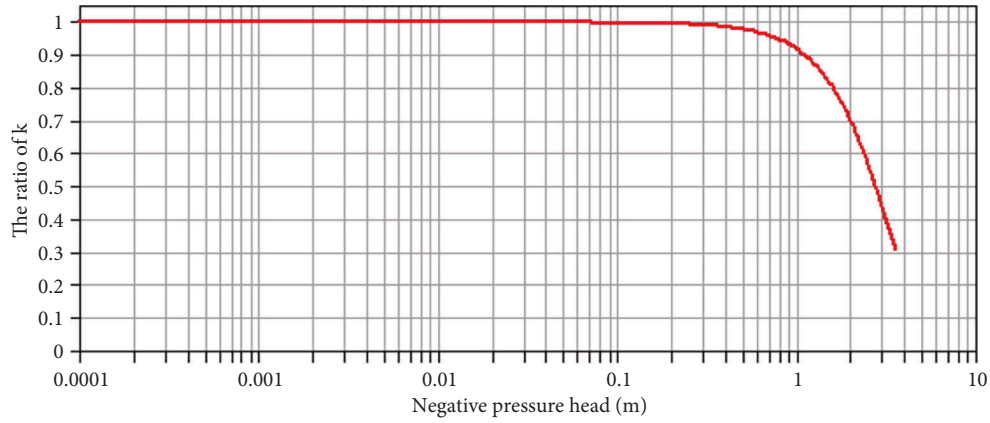

Figure 8: The permeability curve.

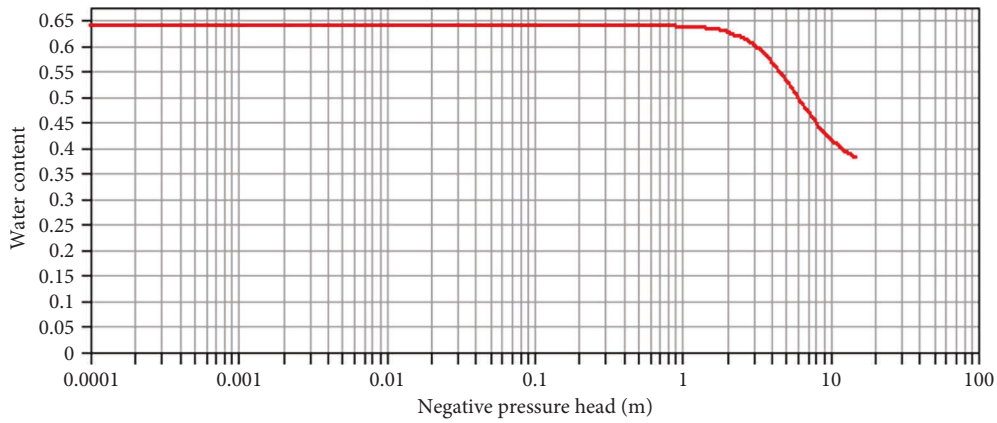

Figure 9: Curve of soil and water characteristics.

where θ is the volume water content of soil; h is the pressure head; and θ_r and θ_s represent residual volume water content and saturated volume water content of the soil, respectively. a, n are empirical fitting parameters. In this paper, $\theta_r = 0.35$, $\theta_s = 0.64$; $a = 0.2$, $n = 3$, $m = 0.66$.

When establishing the rainfall conditions of the model, the influence of the initial groundwater level should be fully considered. In this paper, the pressure head is set to 0 by the operation of the node head. The whole slope surface of the model is set as the rainfall infiltration surface, and the heavy rain lasting 24 hours is taken as the short-term heavy rainfall condition. For the setting of rainfall intensity, the curved flow rate is adopted, and the rainfall intensity is 300 mm/d. Finally, the 8-hour period is divided into three stages for calculation and analysis. The model is shown in Figure 10.

The results show that the slope safety factor decreases to 0.95 after 24 hours of rainfall infiltration, and the slope is extremely unstable. The deformation characteristics of the slope are basically the same as those without rainfall. As far as the deformation degree is concerned, as shown in Figure 11, the initial displacement of the slope has nearly doubled compared with that without rainfall, and the maximum displacement at the slope has reached 0.222 m. The position of the circular slip surface has no significant change compared with that without rainfall, but the damage to the plastic zone has deepened. As shown in Figure 12, the maximum plastic strain changes from 0.0322 to 0.0768, with an increase of 138%. The contour map of pore water pressure before and after rainfall is set by the ISO standard value surface, and the contour map before and after rainfall is shown in Figure 13. Compared to the pore water pressure before and after rainfall, it is found that after 24 h, the water level in the slope increases obviously, and the pore water pressure also increases.

Generally speaking, rainfall infiltration will seriously affect the deformation of rock and soil mass, thus affecting the stability of the slope. The influence of rainfall should be fully considered in slope excavation design and reinforcement optimization.

4. Slope Reinforcement and Results

4.1. Selection of Slope Reinforcement Scheme

4.1.1. Design of Reinforcement Measures. Through calculation, it is found that the safety factor of the slope after excavation is less than 1, the displacement and deformation of the slope are large, and the state is extremely unstable. After the rainfall, the stability safety factor of the slope decreased, the slope damage deepened, and the deformation became more serious. In view of the above situation, reinforcement measures should be taken for the slope. According to the above analysis of the deformation mechanism and failure characteristics of the slope, it is decided to adopt measures such as anchor lattice beam, anchor cable frame beam, and shotcrete for reinforcement. See Table 3 for specific reinforcement measures and Figure 14 for reinforcement effects.

4.1.2. Reinforcement and Protection Structure Design

(1) Roof bolt. The diameter of the bolt hole is 110 mm, and the bolt is made of an HRB400 steel bar of ϕ28 mm. The anchor is 8.5 m long, and the designed pullout resistance is 60 kN. The anchor is 11.5 m long, and the designed pullout force is 90 kN. The grouting body adopts M30 cement slurry. The grouting method is adopted at the bottom of the hole. It is forbidden to pull up the bound PVC grouting pipe in the grouting process. The grouting pipe must not be reused. After grouting is finished, grout should be replenished at the orifice. M30 cement slurry is used for grout replenishment, and a rust inhibitor is added to the M30 cement slurry. Figure 15 shows the reinforcement schematic diagram.

(2) Prestressed anchor cable. The prestressed anchor cable body is made of ordinary prestressed steel strands with ϕ15.2 mm standard tensile strength of 1860 MPa and high strength and low relaxation. The anchor cable body adopts 4 strands of steel strands, and the anchor cable drilling hole is ϕ130 m in diameter, with a designed tensile force of 400 kN and a locking tension of 480 kN; 5~6 bundles of steel strands are used for the anchor cable body,

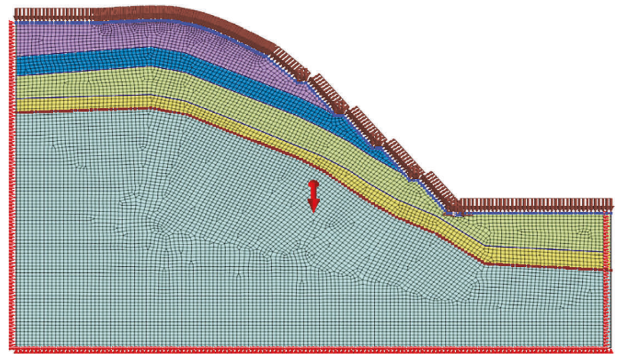

Figure 10: Model diagram under rainfall conditions.

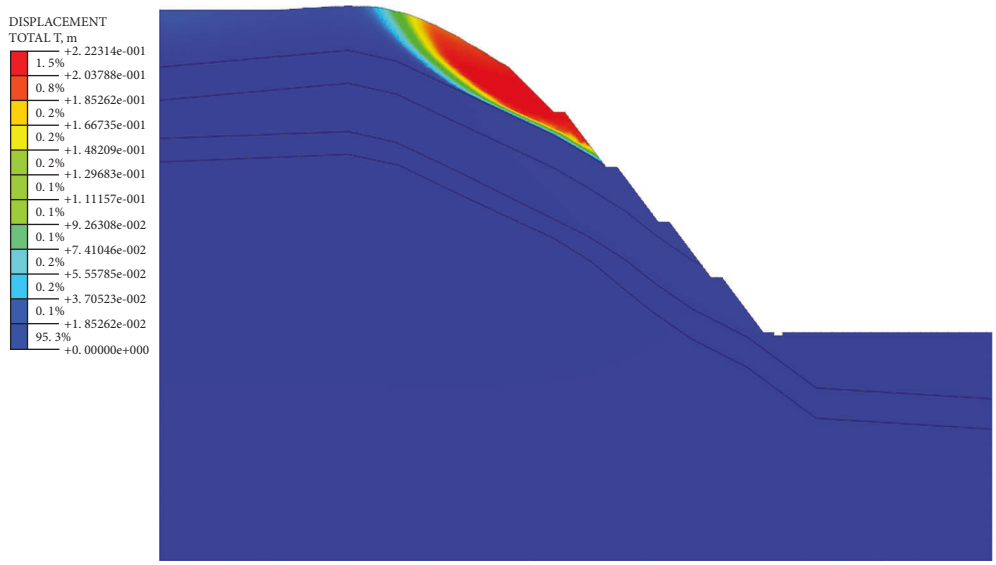

Figure 11: Slope displacement contour under unsupported rainfall conditions.

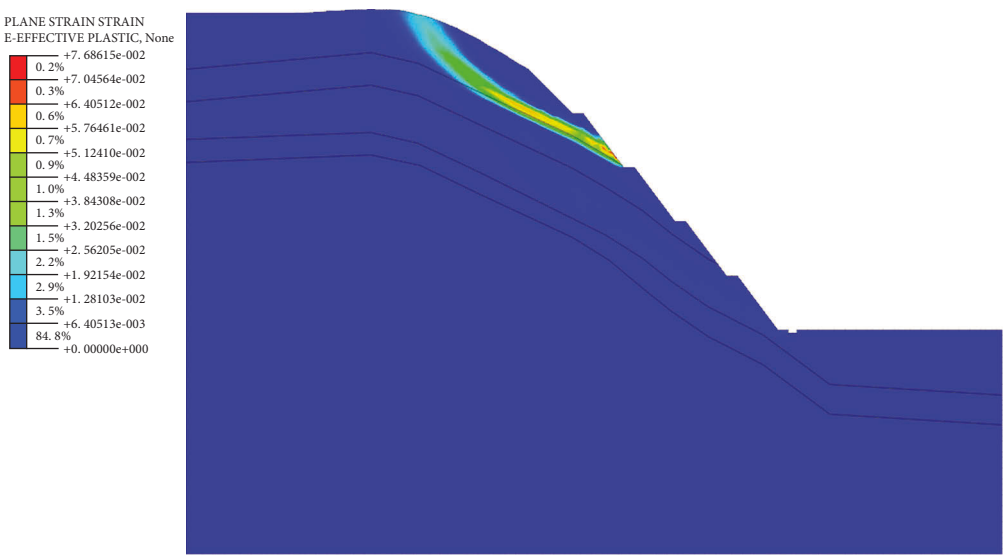

Figure 12: Contour of the effective plastic strain of slope under unsupported rainfall conditions.

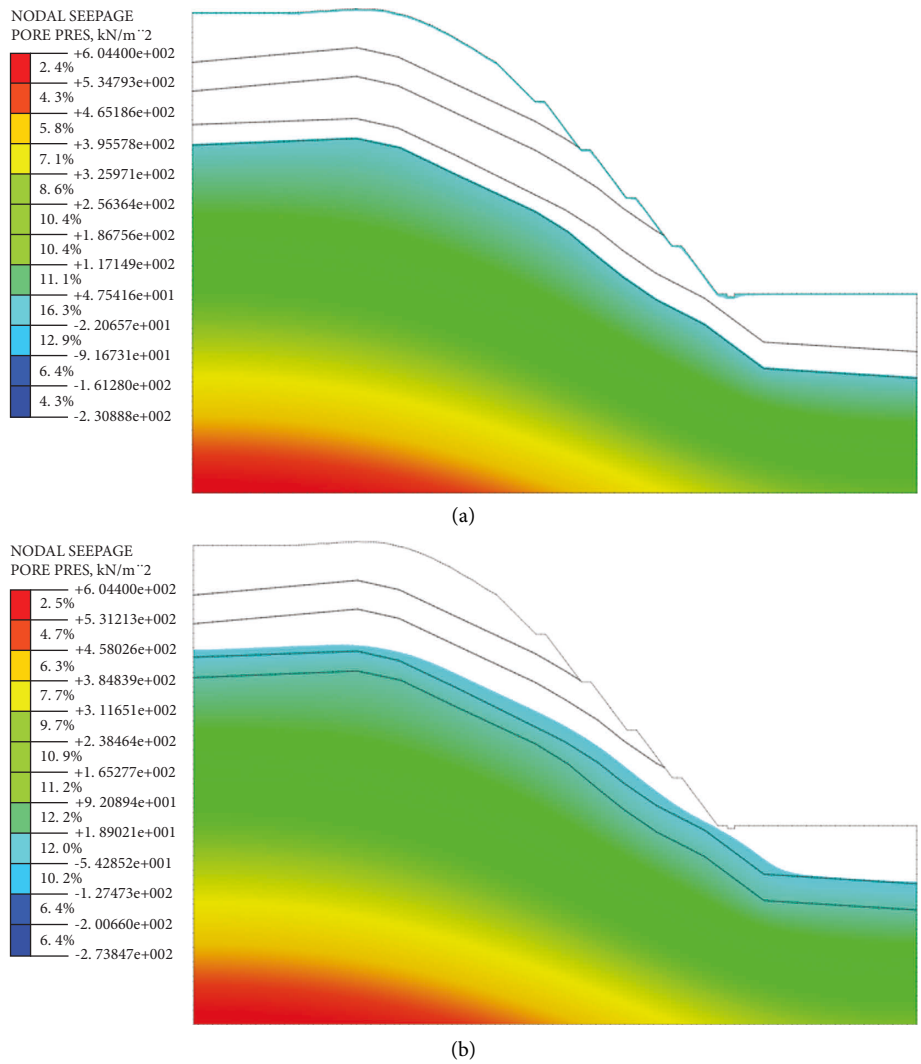

Figure 13: Isograph of pore water pressure of slope before and after rainfall. (a) Before the rainfall. (b) After 24 hours of rain.

Table 3: Slope reinforcement measures.

Slope level	Reinforcement measures
The 1st slope stage	Four anchor bars are used for reinforcement, and the length of the anchor bars is 8.5 m;
The 2nd slope stage	Three prestressed anchor cable frame beams are used for reinforcement, with an anchor cable length of 22 m and anchor cable length of 10 m;
The 3rd slope stage	Three prestressed anchor cable frame beams are used for reinforcement, with an anchor cable length of 26 m and anchor cable length of 10 m;
The 4th slope stage	Three prestressed anchor cable frame beams are used for reinforcement, the anchor cable is 28 m long, and the anchor length is 10 m long;
The 5th slope stage	Four anchor bars are used for reinforcement, and the length of the anchor bars is 11.5 m;

the diameter of the anchor cable drilling hole is ϕ150 mm, the design tension of the anchor cable is 500 kN, and the locking tension is 600 kN. The anchorage length is 10m, secondary grouting is adopted, and cement slurry with a strength of M40 is poured. The primary grouting pressure is not less than 0.5~1.0 MPa, and the secondary grouting pressure is not less than 1.5~2.0 MPa. The reinforcement effect is shown in Figure 16.

(3) Others. The cross-section size of the anchor beam is 0.3×0.3 m, and that of the anchor cable frame beam is 0.4×0.4 m. C30 concrete is used for pouring, and each beam is 6 m long. Expansion joints are set between beams during

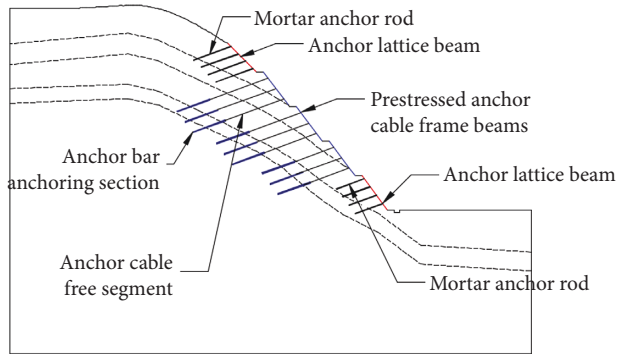

Figure 14: Slope support diagram.

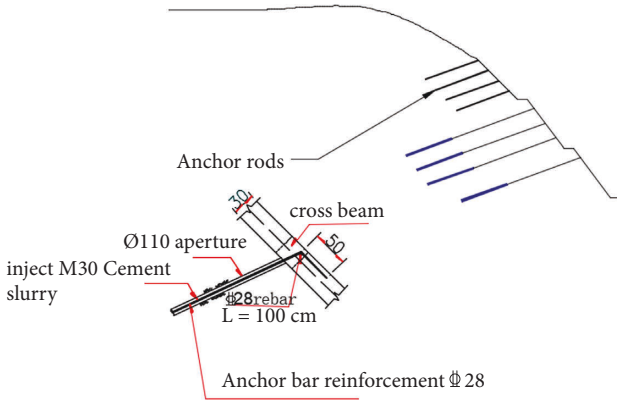

Figure 15: Effect diagram of bolt support.

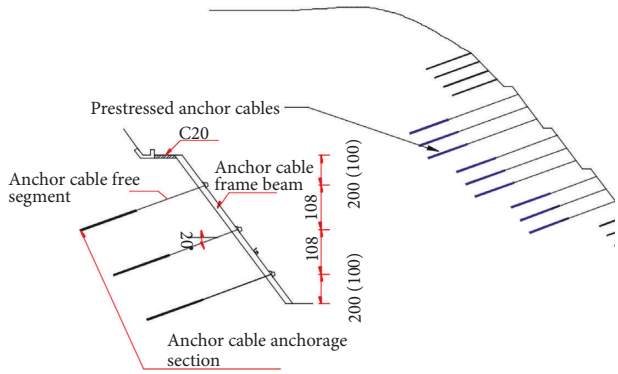

Figure 16: Anchor cable support diagram.

construction. Figure 17 and Figure 18 show the reinforcement effect.

4.2. Application of the Finite Element Method in Slope Reinforcement. The Midas simulation support measures are adopted, and the modified Mohr–Coulomb constitutive model is still adopted for rock and soil. The elastic constitutive model is adopted for the supporting material. The concrete unit type is 1 d slab, the cross-section is a solid rectangle, the anchor rod and anchor cable are 1 d embedded truss, the cross-section is round, and the supporting material attribute parameters are shown in Table 4. An anchor grid beam and an anchor cable frame beam cannot be simulated separately, so they are converted into concrete in the process of numerical simulation.

After grid division, the new model is divided into 11404 units and 11558 nodes, and the whole in-situ stress constraint, dead weight, and prestress are added. Through the anchor modeling assistant, support measures such as anchor rods and anchor cables are added to the model. The angle between the anchor rod and anchor cable and the horizontal

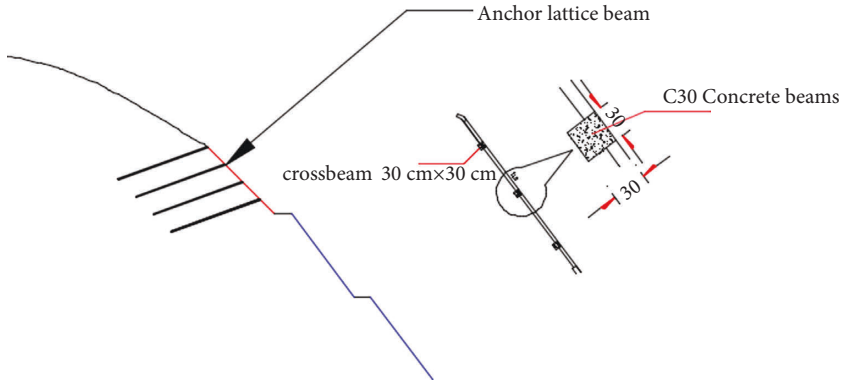

Figure 17: Anchor grid beam support diagram.

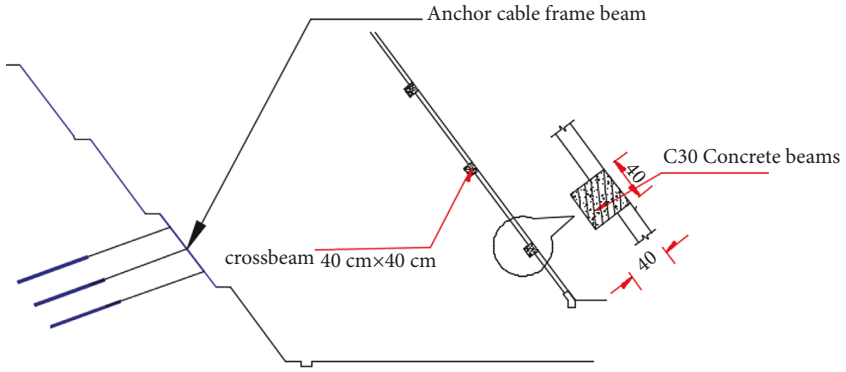

Figure 18: Anchor cable frame beam support diagram.

Table 4: Property parameters of supporting materials.

Material type	Constitutive model	Young's modulus (kN/m^2)	Poisson's ratio	unit weight (kN/m^3)
C30	Elastic	3.0e + 07	0.21	23
C20	Elastic	2.55e + 07	0.2	23
Anchor and anchor cable	Elastic	2.0e + 08	0.3	78

plane is 200°. The grid diagram after support is shown in Figure 19. After the model is established, SRM is used for calculation in the construction stage.

4.3. Stability Analysis of Reinforcement Scheme

4.3.1. Stability Analysis of a Rainless Slope. Numerical simulation based on the SRM principle calculates that the stability safety factor of the slope under support measures is 1.18. Figure 20. The anchoring effect of the slope is obvious; the slip zone almost disappears. As shown in Figure 21, the displacement deformation is reduced to the allowable range, and the landslide deformation is controlled. The maximum displacement deformation is located at the slope shoulder, and the displacement value is 0.034 m.

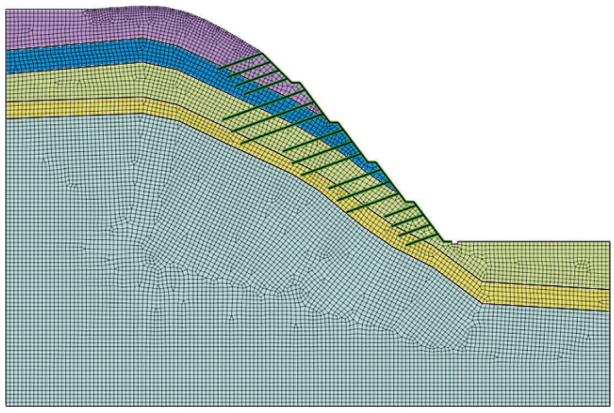

Figure 19: The model after support.

4.3.2. Analysis of the Influence of Rainfall Stability on Slope. Applying the above boundary conditions related to rainfall to the reinforced model and repeating the above operations, the safety factor of slope stability is calculated to be 1.15. According to the research, it is found that the slope soil is strengthened after support, and the influence of rainfall on the stability of the slope is reduced. After support, the

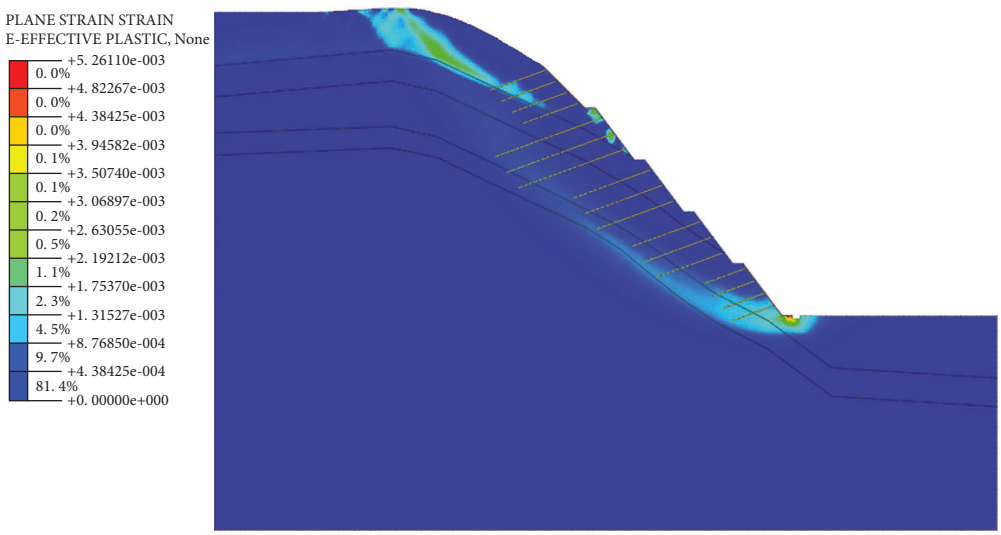

Figure 20: Contour of the effective plastic strain of slope behind support.

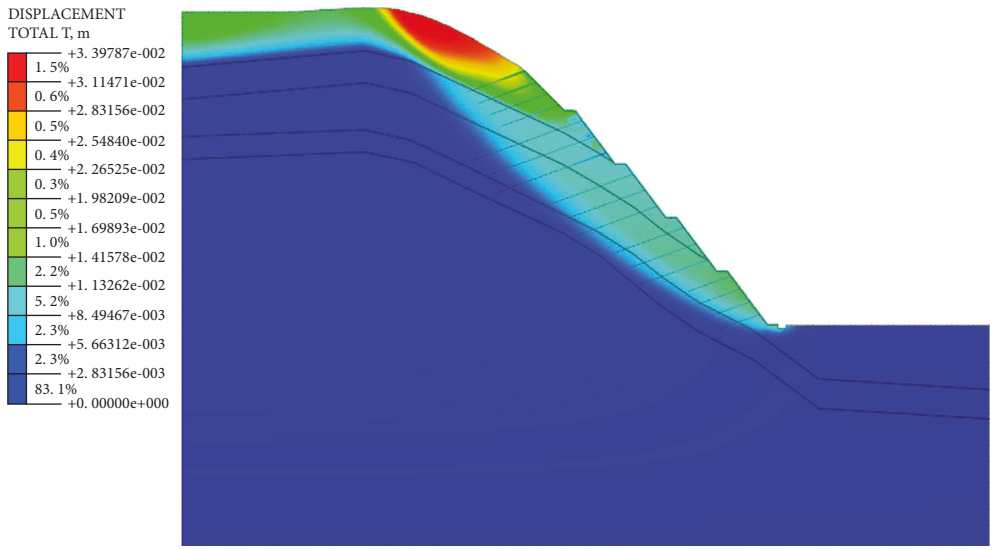

Figure 21: Contour of slope displacement after support.

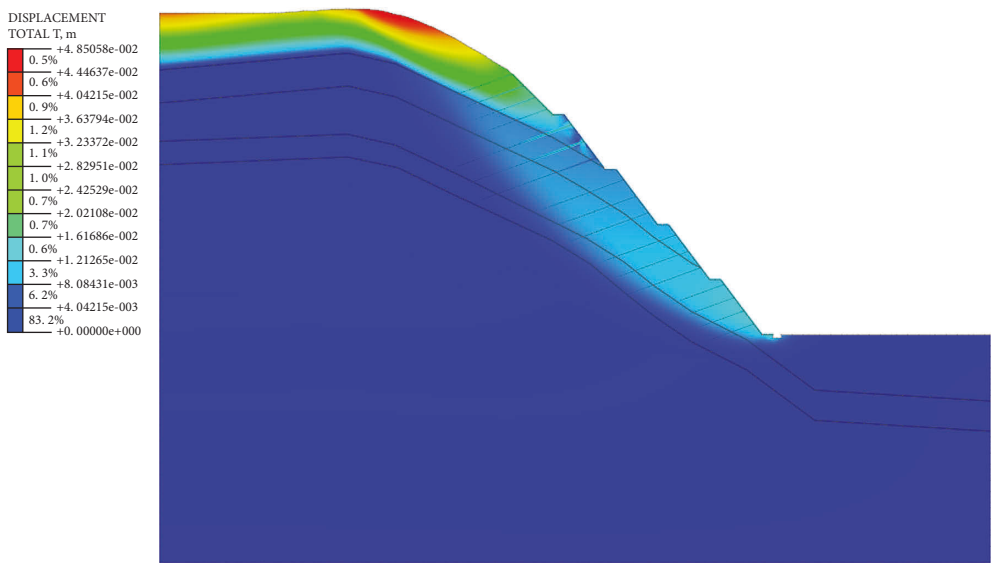

Figure 22: Contour of slope displacement under rainfall condition after support.

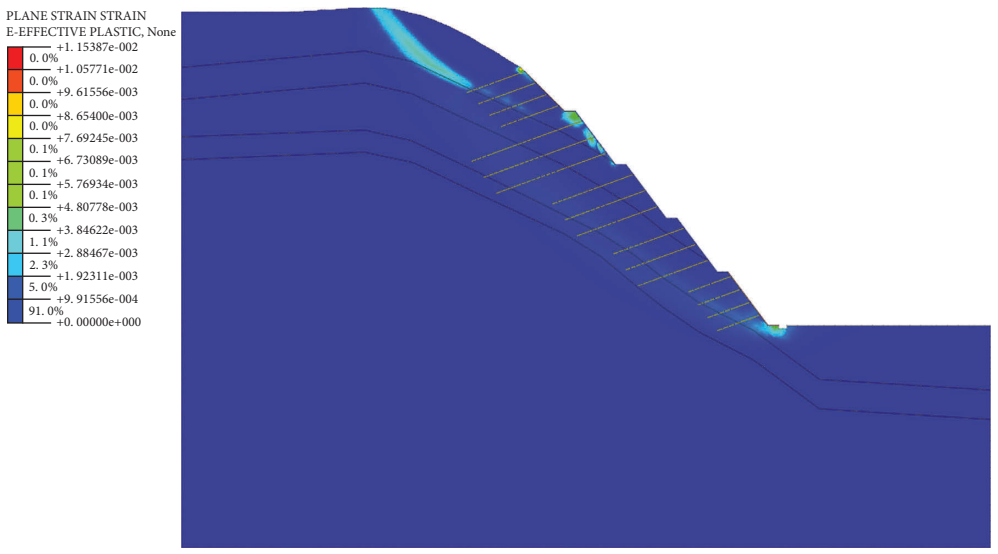

Figure 23: Contour of the effective plastic strain of slope under rainfall condition after support.

maximum displacement of the slope under rainfall conditions is 0.0485 m, which is 78.1% lower than that of the slope without support, which is 0.222 m. Figure 22 provides detailed note. In Figure 23, it can be seen that there is still no slip zone after the slope is reinforced, even under the rainstorm condition, which shows that the reinforcement effect is very ideal.

5. Conclusions

The main conclusions of the thesis are as follows:

(1) The stability safety factor of the slope under natural conditions is 1.05, and the slope is basically stable. After the excavation of the slope, due to the large excavation volume and the large adjustment of the Earth stress after the excavation of the slope body, it is easy to form a large relaxation zone, which leads to the reduction of the stability of the slope, and the stability safety factor is reduced to 0.97, making the whole slope in an unstable state.

(2) The rainstorm conditions have a great influence on the stability of the slope, and the safety factor decreases to 0.95 under the rainstorm conditions after excavation, the slope displacement deformation increases by 98%, the damage to the plastic zone is also deepened, and the maximum plastic strain value increases by 138%. Under these conditions, the plastic area is prone to slope diseases such as collapse and ditching along the structural surface, so it is necessary to strengthen the rainfall slope in time.

(3) With reference to the deformation mechanism, failure characteristics, and geological conditions of the slope, it is proposed to adopt an anchor grid beam and an anchor cable frame beam to reinforce the slope surface.

(4) Through numerical simulation of the reinforced slope, it can be found that the anchorage effect is obvious, the deformation and displacement of the slope are significantly reduced, the slope safety factor is 1.18, and the slope is in a stable state. The safety factor of the slope is 1.15 by simulating the slope under the rainstorm condition after reinforcement. It can be found that even under the rainstorm condition, there is no large deformation, and the slope is still in a stable state.

Data Availability

The data used to support the findings of the study can be obtained from the corresponding author upon request.

Conflicts of Interest

The authors declare that they have no conflicts of interest.

Acknowledgments

This research is sponsored by the doctoral research start-up fund of Hebei GEO University and Hebei University Youth Fund Project (QN202105) and Key Research and Development Projects in Hebei Province (22371701D) and Hebei Province Innovation Ability Promotion Program (21567628H).

References

[1] Z. Li and J. Wang, "Lower bound limit study on plastic limit analysis of rock slope using finite elements based on nonlinear programming," *Chinese Journal of Rock Mechanics and Engineering*, vol. 04, pp. 747–753, 2007.

[2] X. Qiao, "Stability analysis and treatment measures of high slope based on limit equilibrium method," *Railway Engineering*, vol. 57, no. 8, pp. 89–93, 2017.

[3] Y. Wei, L. Jiaxin, L. Zonghong, W. Wei, and S. Xiaoyun, "A strength reduction method based on the Generalized Hoek-Brown (GHB) criterion for rock slope stability analysis," *Computers and Geotechnics*, vol. 117, Article ID 103240, 2020.

[4] H. Wang, B. Zhang, G. Mei, and N. Xu, "A statistics-based discrete element modeling method coupled with the strength reduction method for the stability analysis of jointed rock slopes," *Engineering Geology*, vol. 264, Article ID 105247, 2019.

[5] Y. Yang, G. Sun, H. Zheng, and Y. Qi, "Investigation of the sequential excavation of a soil-rock-mixture slope using the numerical manifold method," *Engineering Geology*, vol. 256, pp. 93–109, 2019.

[6] Z. Nie, Z. Zhang, and H. Zheng, "Slope stability analysis using convergent strength reduction method," *Engineering Analysis with Boundary Elements*, vol. 108, pp. 402–410, 2019.

[7] G. Sun, S. Lin, H. Zheng, Y. Tan, and T. Sui, "The virtual element method strength reduction technique for the stability analysis of stony soil slopes," *Computers and Geotechnics*, vol. 119, Article ID 103349, 2020.

[8] Y. B. Zhou, R. G. Ye, and Y. J. Li, "Targeting the CD134-CD134L interaction using anti-CD134 and/or rhCD134 fusion protein as a possible strategy to prevent lupus nephritis," *Rheumatology International*, vol. 29, no. 4, pp. 417–425, 2008.

[9] G. Chen, R. Huang, Y. Shi, and Q. Xu, "Stability analysis of slope based on dynamic and whole strength reduction methods," *Chinese Journal of Rock Mechanics and Engineering*, vol. 33, no. 02, pp. 243–256, 2014.

[10] P. Su, P. Qiu, B. Liu, W. Chen, and S. Su, "Stability prediction and optimal angle of high slope in open-pit mine based on twodimension limit equilibrium method and three-dimension numerical simulation," *Physics and Chemistry of the Earth*, vol. 127, 2022.

[11] T. Yang, Y. Rao, N. Ma, J. Feng, H. Feng, and H. Wang, "A new method for defining the local factor of safety based on displacement isosurfaces to assess slope stability," *Engineering Geology*, vol. 300, Article ID 106587, 2022.

[12] K. Yang and Y. Zhu, "Soil slope stress state and stability analysis based on unloading effect of slope surfaces," *Engineering Mechanics*, vol. 38, no. 11, pp. 95–104, 2021.

[13] S. Chen, Y. Zhu, Z. Li, L. Huang, and H. Zhang, "Analysis of lateral slope stability during construction of a loess tunnel with a large section," *Modern Tunnelling Technology*, vol. 51, no. 1, pp. 82–89, 2014.

[14] Yu. Zhao, T. Wang, W. Li, and F. Dai, "Stability evaluation and treatment simulation of an expressway landslide," *Chinese Journal of Rock Mechanics and Engineering*, vol. 27, no. 11, pp. 2340–2346, 2008.

[15] Q. Xu, D. Zhang, and G. Zheng, "Failure mode and stability analysis of leet bank abutment high slope at Jinping I hydropower station," *Chinese Journal of Rock Mechanics and Engineering*, vol. 28, no. 6, pp. 1183–1192, 2009.

[16] X. Song and Y. Tan, "Experimental study on failure of temporary earthen slope triggered by intense rainfall," *Engineering Failure Analysis*, vol. 116, pp. 104718–104812, 2020.

[17] C. Sun, A. Li, and H. Zhang, "Numerical simulation on slope stability under rainfall infiltration," *Port Engineering Technology*, vol. 50, no. 4, pp. 67–70, 2013.

[18] J. Tian, L. Han, X. Jin, L. Xu, X. Wang, and Y. Dong, "Effect of rainfall on slope stability of Picea crassifolia forest based on finite element method in Qinghai," *Science of Soil and Water Conservation*, vol. 17, no. 6, pp. 11–18, 2019.

[19] B. Bai, Y. Wang, D. Y. Rao, and F. Bai, "The effective thermal conductivity of unsaturated porous media deduced by pore-scale SPH simulation," *Frontiers of Earth Science*, vol. 10, 2022.

[20] B. Bai, R. Zhou, G. Q. Cai, W. Hu, and G. C. Yang, "Coupled thermo-hydro-mechanical mechanism in view of the soil particle rearrangement of granular thermodynamics," *Computers and Geotechnics*, vol. 137, no. 8, Article ID 104272, 2021.

[21] B. Bai, G. C. Yang, T. Li, and G. S. Yang, "A thermodynamic constitutive model with temperature effect based on particle rearrangement for geomaterials," *Mechanics of Materials*, vol. 139, Article ID 103180, 2019.

[22] L. Chen and X. Jin, "Study on the applicability of three criteria for slope instability using finite element strength reduction method," *China Civil Engineering Journal*, vol. 45, no. 9, pp. 136–146, 2012.

[23] S. Zhao, Y. Zheng, and Y. Zhang, "Study on slope failure criterion in strength reduction finite element method," *Rock and Soil Mechanics*, vol. 26, no. 2, pp. 332–336, 2005.